Supporting Information

WO_x Nanoparticles Coupled with Nitrogen-doped Porous Carbon toward Electrocatalytic N_2 Reduction

Zhaobing Lu [a], Hui Wang [b], Yinghao Tao [b], Sheng Zhu [a*], Weiju Hao [b], Xinjuan Liu[b*], Yulin Min [a], and Jinchen Fan [a, b*]

[a] Shanghai Key Laboratory of Materials Protection and Advanced Materials in Electric Power, College of Environmental and Chemical Engineering, Shanghai University of Electric Power, Shanghai, China

[b] School of Materials and Chemistry, University of Shanghai for Science and Technology, Shanghai, 200093, China

* E-mails: zhusheng@shiep.edu.cn (S. Z.); xjliu@usst.edu.cn (X. L.); jcfan@usst.edu.cn (J. F.)

1. Experimental Section.

1. 1 Indole blue spectrophotometric method for determining the yield of NH_3.

The concentration of synthesized ammonia via the electrocatalytic NRR was determined by the indophenol blue method.[1] In the indophenol blue method, 4 mL of electrolyte was removed from the electrochemical reaction vessel after the electrolysis process and added into 50 μL of oxidant (NaClO + NaOH), 500 μL of colorant ($C_7H_5O_3Na$ + NaOH), and 100 μL of catalyst ($Na_2[Fe(CN)_5NO]\cdot 2H_2O$). After standing in darkness for 2 h at room temperature, the absorption spectrum was measured using a UV−vis spectrophotometer. The formation of indophenol blue was determined using the absorbance at a wavelength of 698 nm. The concentration−absorbance curves were calibrated using standard solutions: 0.1 M Na_2SO_4 electrolyte with a series of concentrations of NH_4Cl. The standard curve was plotted with the absorbance values at a wavelength of 698 nm as the y axis and the concentration of NH_3 as the x axis. The obtained standard curve (y = 0.09143x -0.00243, R^2 = 0.999) shows a good linear relationship of the absorbance value with NH_3 concentration.

The yield of NH_3 could be calculated according to the Equation 1,

$$R(NH_3)\ (mg\ h^{-1}\ mg^{-1}) = \frac{C(NH4^+ - N)(\mu g\ mL^{-1}) \times V(mL) \times 17}{t(h) \times m(mg) \times 14}\ , \text{(Equation 1)}$$

$R(NH_3)$ is the yield of NH_3 (mg❿h^{-1}❿mg^{-1}).

V is the total volume of electrolyte solution for NRR reaction.

C_{NH4^+-N} is 14 (g mol^{-1}).

t is reaction time (h).

17 is the molar mass value of NH_3.

m is the load of catalyst on the working electrode (mg).

1.2 Determination of FE.

The faradaic efficiency (FE) was determined using the following Equation 2.

$$FE(NH_3)\ (\%) = \frac{3 \times n(NH3)(mol) \times F}{Q} \times 100\%\ , \text{(Equation 2)}$$

FE is Faraday efficiency.

F is Faraday constant (96485.34).

Q is the total electric charge during NRR reaction.

1.3 Watt and Chrisp method for determining the concentration of hydrazine.

The content of hydrazine (N_2H_4) in the electrolyte was measured by the method of Watt and Chrisp.[2] The hydrazine color reagent was prepared by dissolving 5.99 g of p-dimethylaminobenzaldehyde (p-$C_9H_{11}NO$) in

the mixture of 30 mL of concentrated HCl and 300 mL of ethanol. Three milliliters of the above prepared color reagent were added into 5 mL of electrolyte and then was stirred for 10 min at room temperature in darkness. The absorbance of hydrazine in the resulting electrolyte was estimated at 460 nm. After that, the UV-Vis absorption curve for the above mixture solution was recorded. The concentration of N_2H_4(x) were calculated from the absorbance (y) at the maximum absorption wavelength of λ_{max}=455 nm according to the lambert-beer law.[3] The concentration–absorbance curve was calibrated by using standard ammonia solutions at a series of concentrations, and the fitting curve is y = 0.020936x-0.00168, (R^2 = 0.9999).

1.4 Preparation of working electrode

1 mg catalyst were dispersed in 900 μL of ethanol and 100 μL of Nafion solution to form a homogeneous catalyst ink under sonication for 30 min. Then, 100 μL of catalyst ink were dropped evenly on carbon paper for catalytic area (1×1 cm^2), and dried at room temperature.[4]

1.5 ^{15}N isotope labeling experiment

The $^{15}N_2$ isotopic labeled experiment was carried out using the $^{15}N_2$ isotope as the feeding gas to determine the N source of ammonia.[5] Before electrolysis, ultrahigh-purity Ar (99.999%) was purged for 30 min to remove O_2 and N_2. Then $^{15}N_2$ was prepurified by flowing through 0.05 M H_2SO_4 solution to remove N contamination and purged for 30 min to saturate the electrolyte. After electrolysis at -0.75 V (vs. RHE) for 2 h in 0.1 M Na_2SO_4 solutions, the resulting electrolyte was concentrated by hearting at 80 ℃. The analysis of $^{15}NH_3$ product was conducted by the ^{1}H NMR with d^6-DMSO.

1.6 Density functional theory (DFT) calculation details

All theoretical calculations were performed using the density functional theory (DFT), as implemented in the Material Studio Dmol3. The electron exchange and correlation energy functions were treated using the generalized gradient approximation, as captured using the Perdew-Burke-Ernzerh functional (GGA-PBE). Iterative solutions of the Kohn-Sham equations were done using a plane-wave basis set defined using a kinetic energy cutoff of 500 eV.[6] The k-point sampling was obtained from the Monkhorst-Pack scheme with a (1 × 1 × 1) mesh. The convergence criteria for the electronic self-consistent iteration and force were set to 1 × 10^{-5} eV and 0.001 eV❿$Å^{-1}$, respectively. Van der Waals's force was corrected by DFT-D3.

The catalytic activities of the WO_x/NPC and the WO_2 (011) surface were evaluated by the Gibbs free energy calculations. In the standard computational hydrogen electrode model, the Gibbs free energy change of an elementary step along a reaction pathway can be written as $\Delta G = \Delta E + \Delta E_{ZPE} - T\Delta S + \Delta G_U + \Delta G_{pH}$. ΔE is the reaction energy between the products and the reactants of the elementary step, which is corrected by the change in the zero-point energy (ΔE_{ZPE}) and the vibrational entropy (ΔS) at T=298.15k. ΔG_U = eU is the Gibbs free

energy correction from the applied electrode potential , only for the elementary step involving electron-proton coupling/de-coupling.[7] These values of each adsorbed state were obtained from DFT calculation, whereas that of gas molecules were from standard tables (see Table S3) $\Delta G_{PH} = \kappa_B T \times pH \times \ln 10 = 0.059 \times pH$ is the correction from pH which is set to 0 under the standard condition. The potential-determining step (PDS) along a reaction pathway is the one having the largest ΔG (ΔG_{max}) and the limiting potential is calculated as $U_{limiting} = -\Delta G_{max}/e$. It should be noted that the NRR active sites of the WO_2 (011) surface were identified by iteratively testing all surface sites.[8]

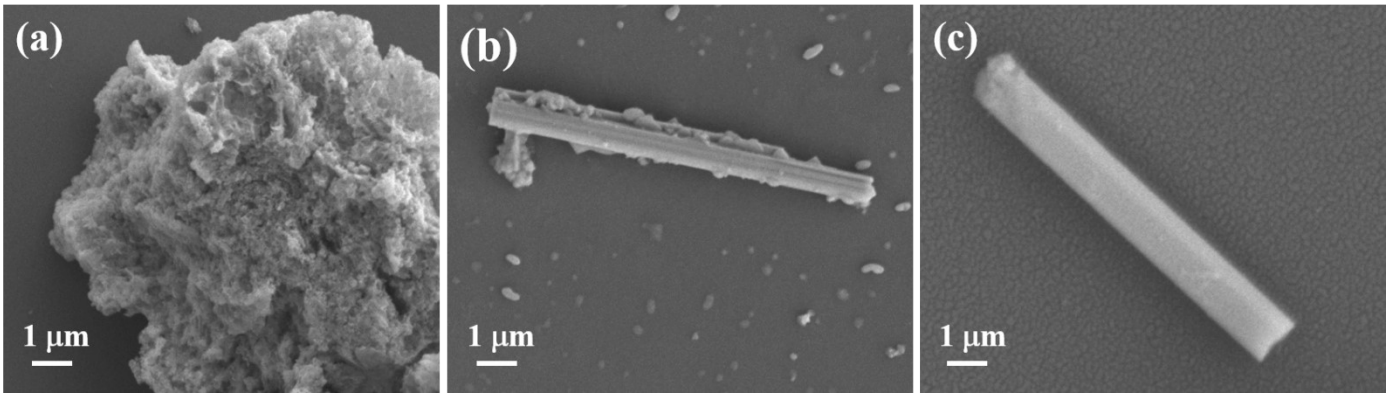

Figure S1. Scanning electron microscopy (SEM) images of (a) WO_x/NPC-700 ℃, (b) WO_x/NPC-800 ℃ and (c) WO_x/NPC-900 ℃.

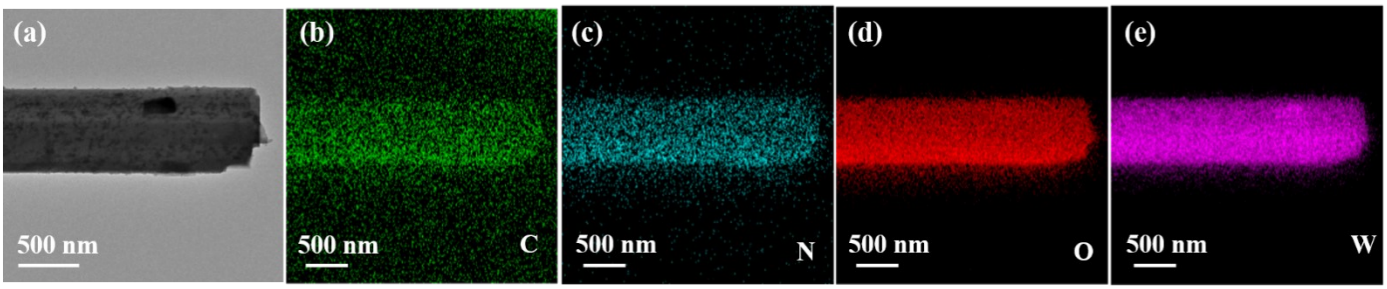

Figure S2. SEM image of (a) WO_x/NPC-900 ℃, (b-c) corresponding elemental mapping images of WO_x/NPC-900 ℃.

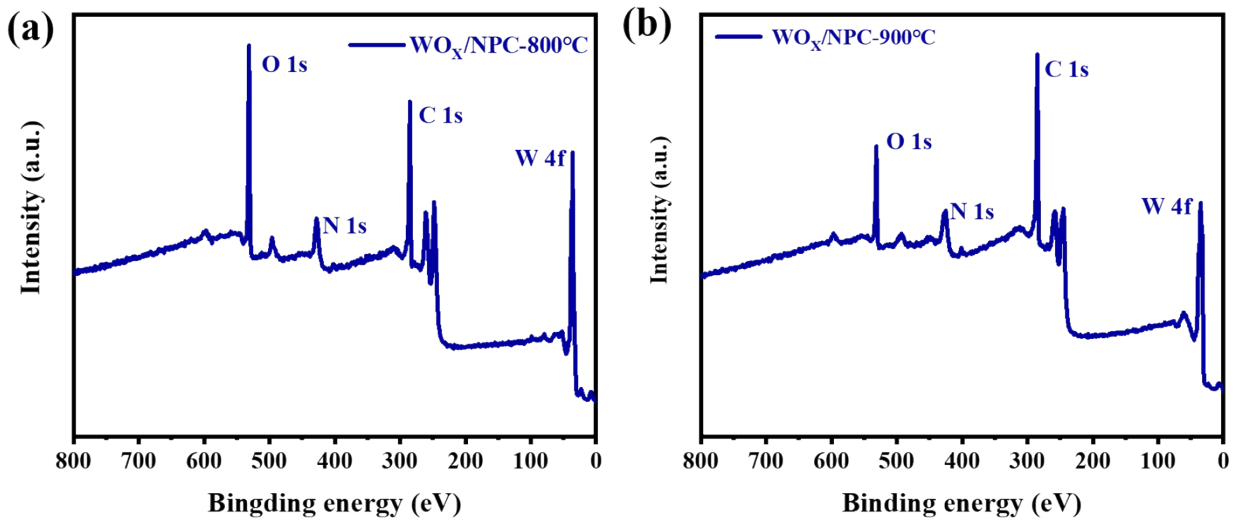

Figure S3. X-ray photoelectron spectroscopy (XPS) survey spectra of (a) WO_x/NPC-800 ℃ and (b) WO_x/NPC-900 ℃.

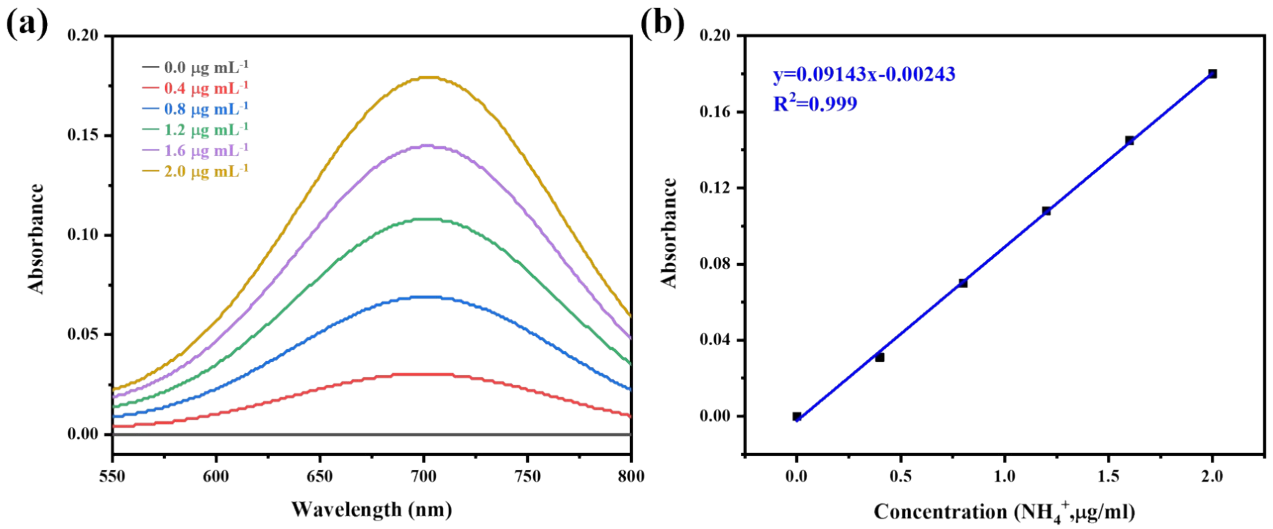

Figure S4. Calibration curve of the indophenol blue method in 0.10 M Na_2SO_4 using NH_4Cl solutions with specific concentration as standards. (a) UV-vis curves of indophenol assays with different concentrations of NH_3 after incubated for 2 hours and (b) calibration curve used for determining NH_3 concentration. The absorbance at 698 nm was measured by a UV-vis spectrophotometer, and the fitting curve shows good linear correlation of absorbance with NH_3 concentration (y=0.01943x-0.00243, R^2=0.999).

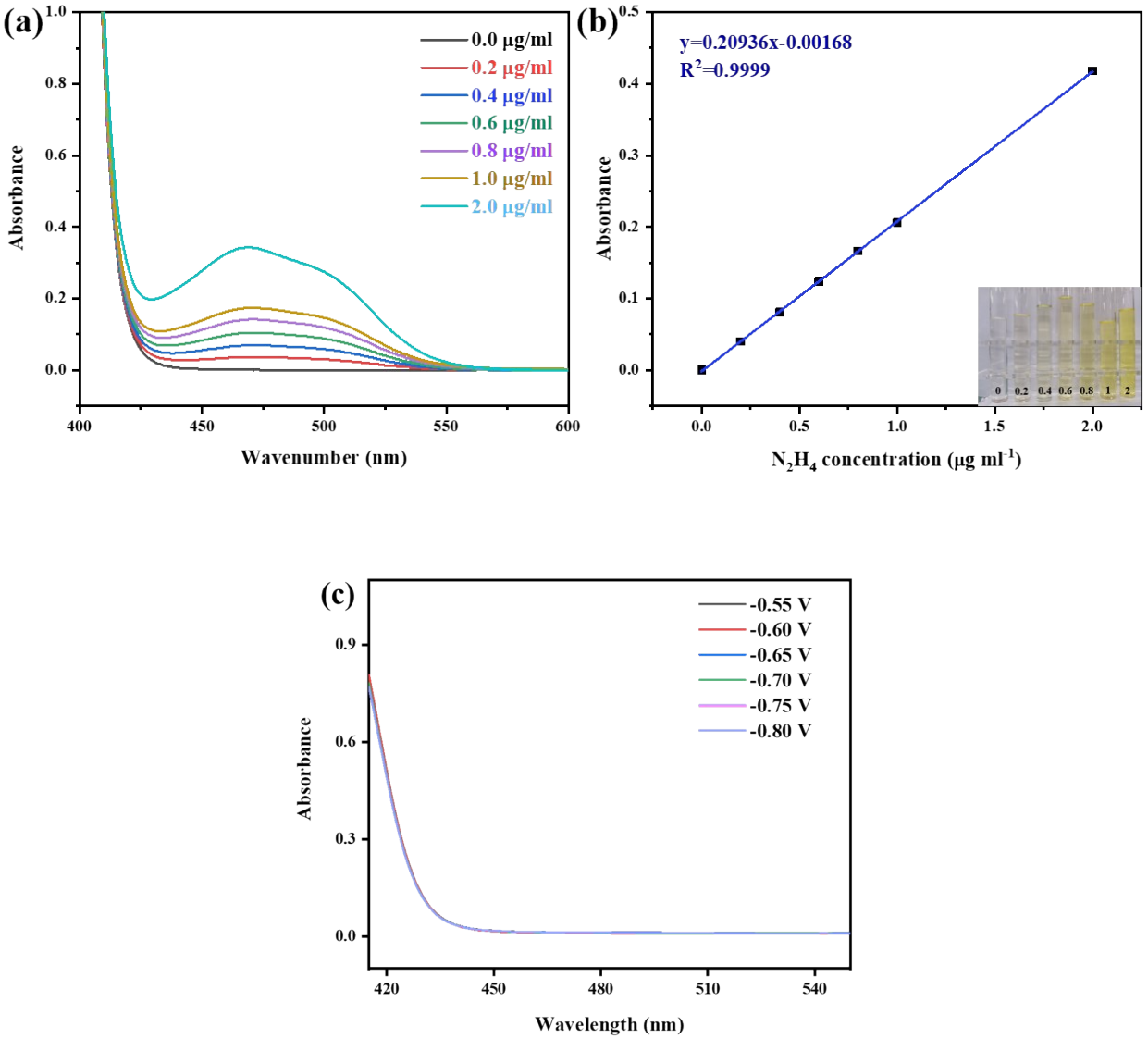

Figure S5. Calibration for N_2H_4 detection using the Watt and Chrisp method. (a) UV-vis curves of different concentrations of N_2H_4 stained with the color indicator and incubated for 10 min and (b) calibration curve used for estimation of N_2H_4 concentration. The absorbance at 455 nm was measured by a UV-vis spectrophotometer, and the fitting curve shows good linear correlation of absorbance with N_2H_4 concentration. (y = 0.020936x-0.00168, R^2 = 0.9999). (c) UV-vis absorption spectra of the electrolytes stained with N_2H_4 color indicator after electrocatalytic NRR on WO_x/NPC-700 ℃ catalyst at different potentials.

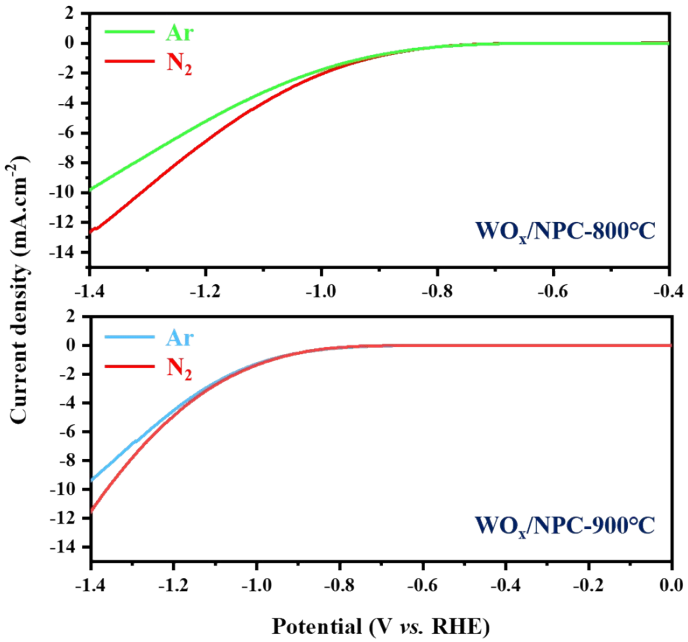

Figure S6. Linear sweep voltammetry (LSV) curves of WO_x/NPC-800 ℃ and WO_x/NPC-900 ℃ in N_2 and Ar saturated 0.10 M Na_2SO_4 electrolyte.

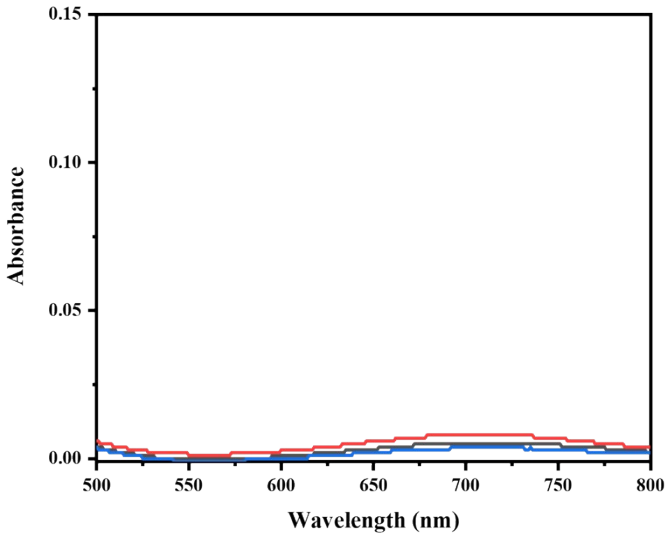

Figure S7. The UV-Vis absorption curves of the WO_x/NPC-700 ℃ under different conditions (red line: blank N_2-saturated 0.1M Na_2SO_4 electrolyte, black line: electrolysis in Ar-saturated 0.1M Na_2SO_4 electrolyte, and blue line: react under open circuit).

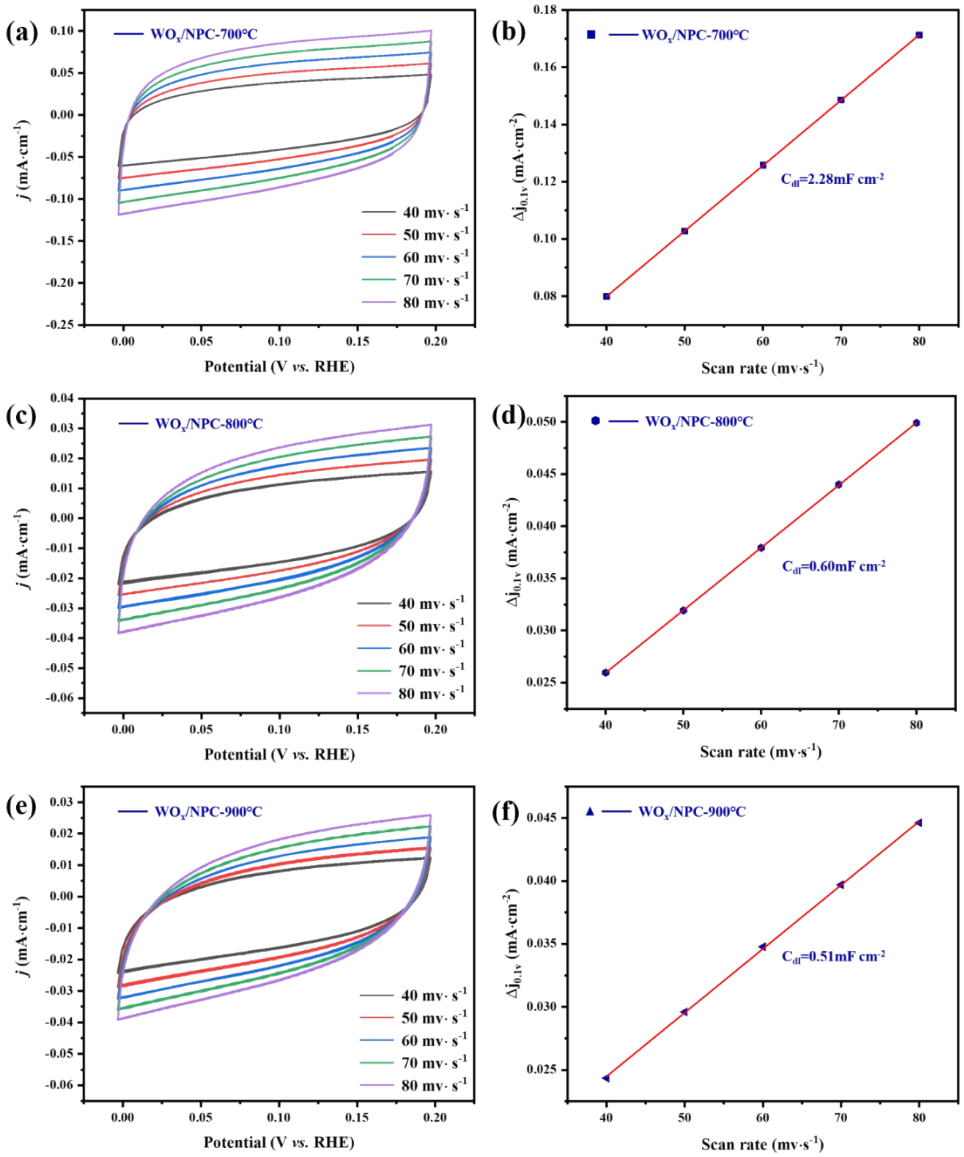

Figure S8. Electrochemical double-layer capacitance measurements: CV curves of (a) WO_x/NPC-700 ℃ (c)WO_x/NPC-800 ℃, (e) WO_x/NPC-900 ℃ catalysts from 40mV to 80mV with different scan rates. (b) (d) (e)The corresponding linear fitting of the current density versus scan rates.

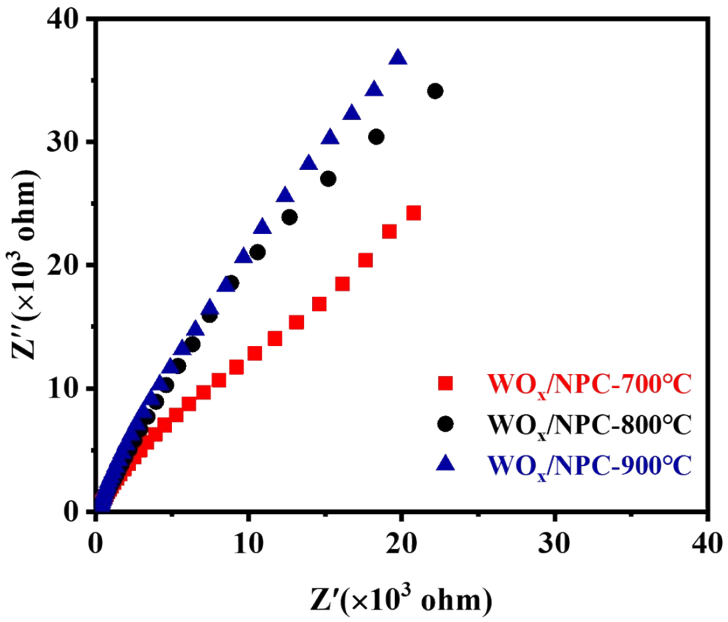

Figure S9. Electrochemical impedance spectroscopy (EIS) plots of the WO_x/NPC-700℃， WO_x/NPC-800 ℃ and WO_x/NPC-900 ℃.

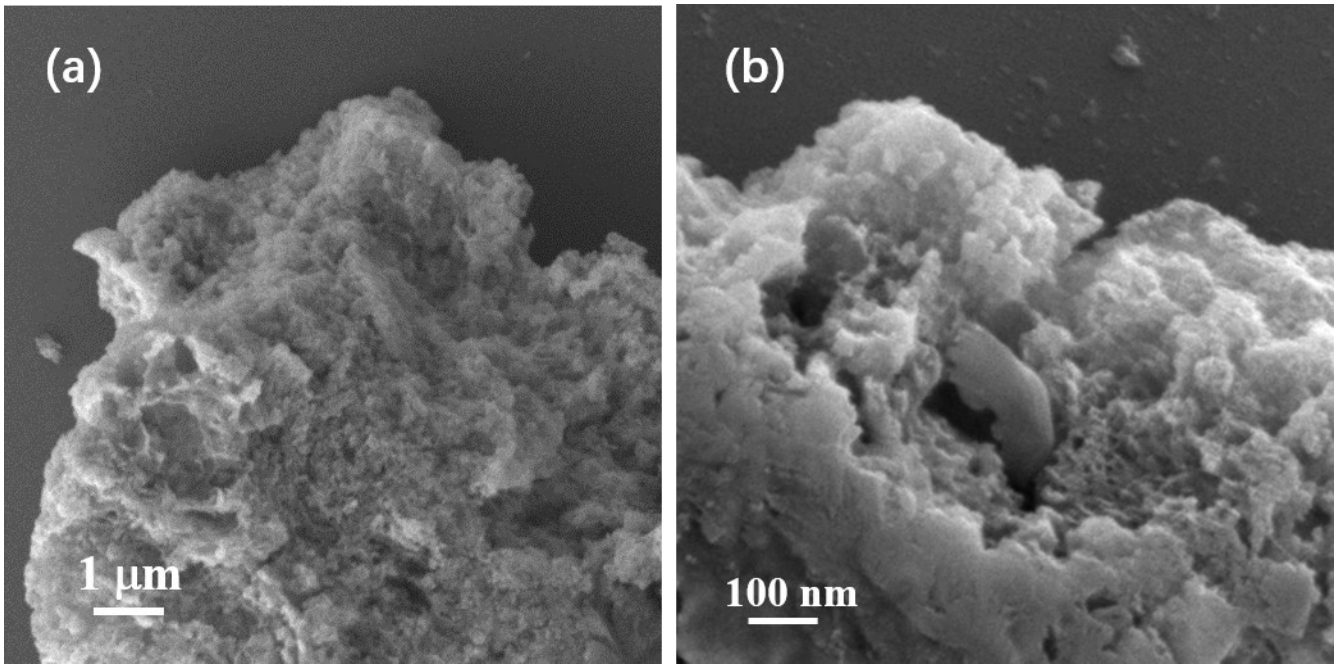

Figure S10. SEM images for the WO_x/NPC-700 ℃ electrocatalyst (a) before and (b) after the eNRR test.

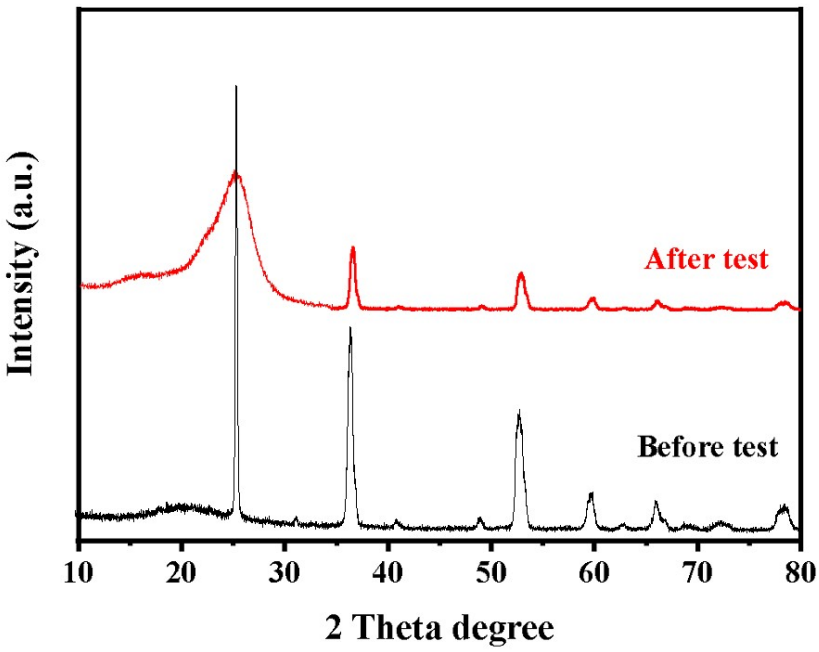

Figure S11. XRD patterns for the WO_x/NPC-700 °C catalyst before and after the eNRR test.

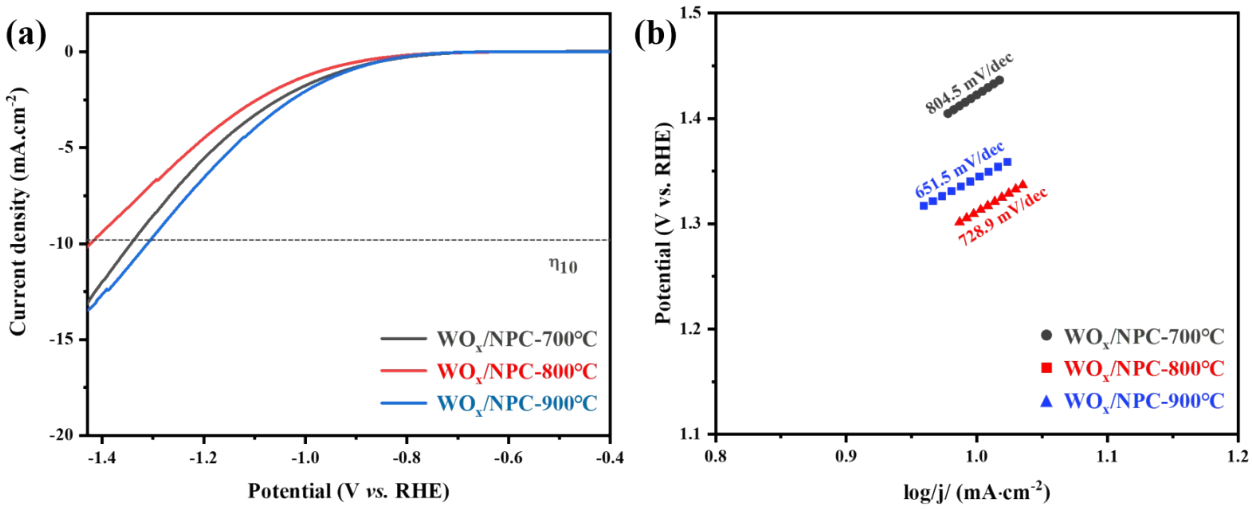

Figure S12. (a) Comparison of polarization curves of WO_x/NPC-700 °C, WO_x/NPC-800 °C and WO_x/NPC-900 °C for HER in Ar-saturated 0.1 M Na_2SO_4 electrolyte. (b) Corresponding Tafel plots derived from polarization curves.

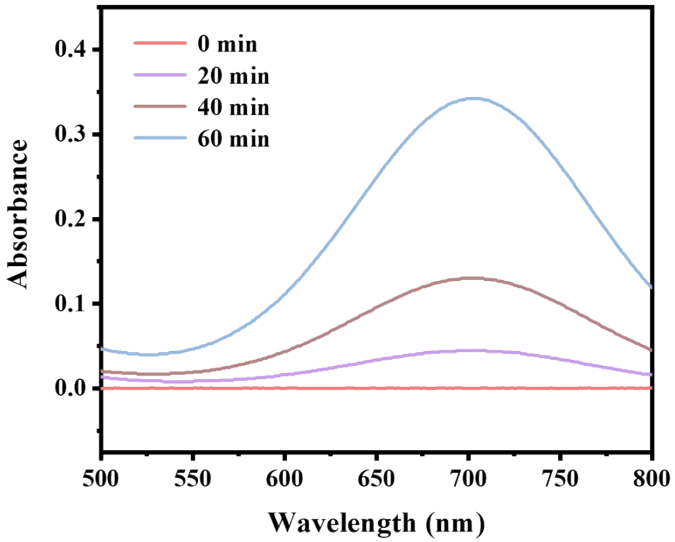

Figure S13. The UV-Vis absorption curves of the 0.1 M Na_2SO_4 electrolytes stained with indophenol indicator after 0 min, 20 min, 40 min and 60 min electrolysis at -0.75 V (*vs.* RHE).

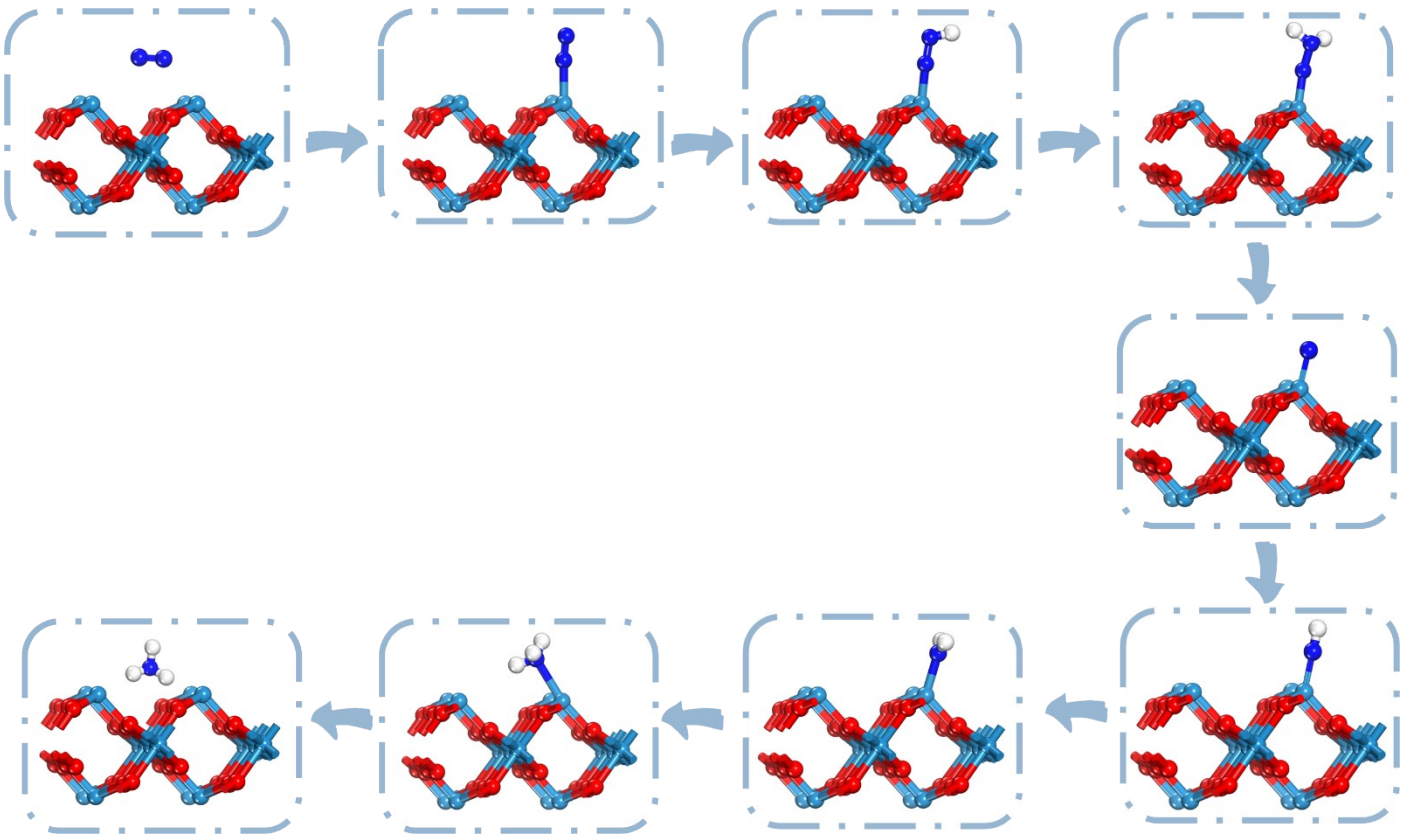

Figure S14. Protonation hydrogenation model of pure WO_2 in nitrogen reduction process. (red:O, blue:N, white:H and ching:W)

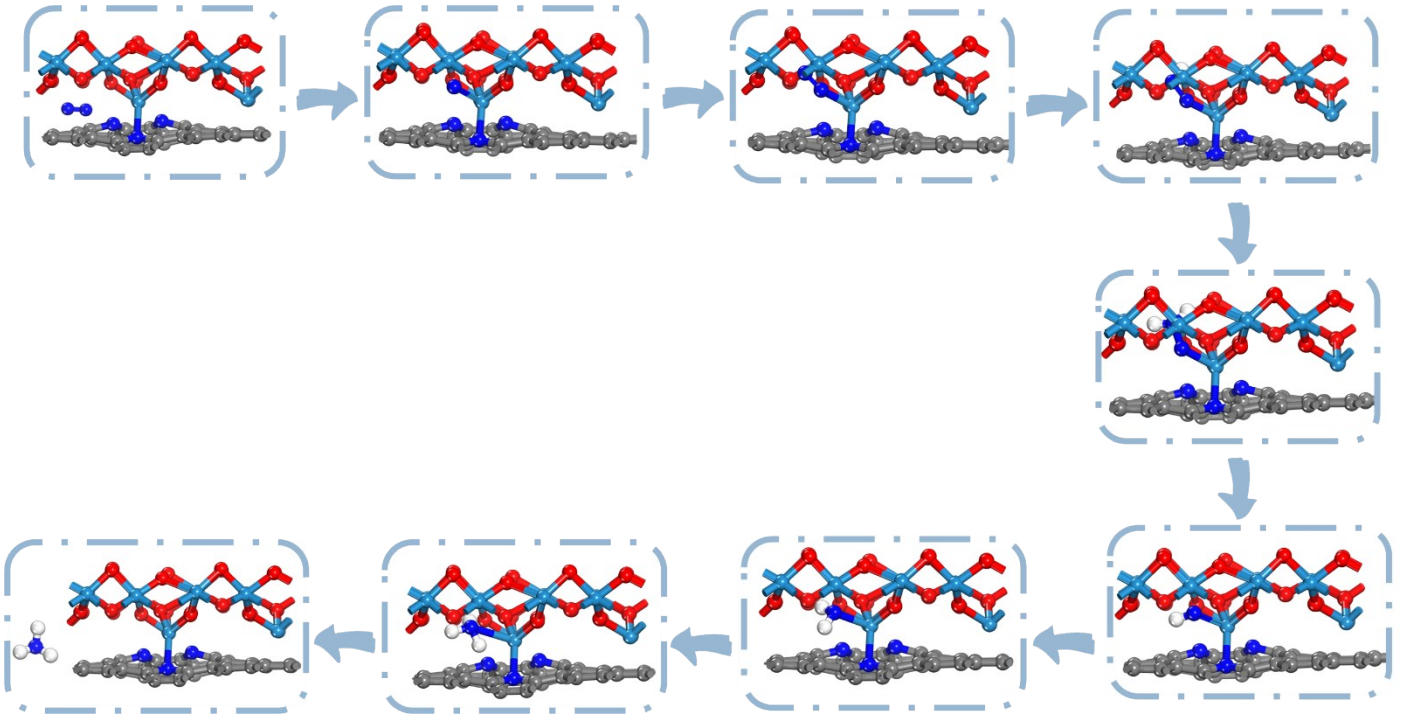

Figure S15. Model diagram of protonation hydrogenation of WO_x/NPC-700 ℃ in nitrogen reduction process. (red:O, blue:N, white:H and ching:W).

Table S1. Surface texture properties of WO_x/NPC-T.

Samples	WO_x/NPC-700 ℃	WO_x/NPC-800 ℃	WO_x/NPC-900 ℃
BET surface area (m^2/g)	150.1387	75.4327	22.1149
Total pore volume (cm^3/g)	0.517444	0.377082	0.079097
Average pore Size (nm)	6.782	8.196	9.571

Table S2. Comparison of electrosynthesis activity of NH_3 catalysts at room temperature.

Catalyst		System	Applied potential V(vs.RHE)	Yield	Faradic Efficiency
W-based NRR catalysts	**WO_x/NPC (This work)**	**0.05 M Na_2SO_4**	**-0.75 V**	**46.8μg$_{cat}^{-1}$h^{-1}**	**10.3%**
	W 2D layered W_2N_3 nanosheet.[9]	0.10 M KOH	-0.1 V	11.66 ±0.98μg$_{cat}^{-1}$h^{-1}	11.67% ± 0.93
	Heterogeneous WS_2/WO_2.[10]	0.05 M H_2SO_4	-0.1 V	8.53μg$_{cat}^{-1}$h^{-1}	13.5%
	W-NO/NC.[11]	0.5 M $LiClO_4$	-0.7 V	12.62μg$_{cat}^{-1}$h^{-1}	8.35%
	WO_{3-x} nanosheets.[12]	0.1 M HCl	-0.3 V	17.28μg$_{cat}^{-1}$h^{-1}	7.0%
N-Doped NRR catalysts	N-Doped Porous Carbon.[13]	0.05 M H_2SO_4	−0.9 V	1.40 mmol g^{-1}h^{-1}	1.42%
	Mo_2C/NC.[14]	0.1 M Na_2SO_4	-0.2 V	70.6 mmol h^{-1}g$_{cat.}^{-1}$	12.3%
	Mo/BCN.[15]	0.10 M KOH	−0.4 V	37.67μg$_{cat}^{-1}$h^{-1}	13.27%

Table S3. Zero point energy and entropy contributions to the free energy of gas phase and adsorbed

species at 298.15 K for the WO_2 (011) (in eV).

WO_2 (011)	**TS**	**ZPE**
N_2	2E-03	0.91
H_2	1.36E-03	0.27
NH_3	2E-03	0.15
*N_2	-5.17E-03	2.08
*NNH	-3.07E-03	2.23
*NNH_2	-1.85E-04	2.44
*NNH_3	-2.00E-05	2.78
*N	-2.97E-03	2.14
*NH	-1.89E-03	2.33
*NH_2	-2.70E-05	2.64
*NH_3	-8.44E-09	3.05

Table S4. Zero point energy and entropy contributions to the free energy of gas phase and adsorbed species at 298.15 K for WO_2/NPC (011) (in eV).

WO_2/NPC (011)	**TS**	**ZPE**
N_2	2E-03	0.91
H_2	1.36E-03	0.27
NH_3	2E-03	0.15
*N_2	-2.57E-05	9.20
*NNH	-2.58E-05	9.42
*NNH_2	-1.61E-05	9.75
*NNH_3	-7.58E-06	10.09
*N	-2.58E-05	9.29
*NH	-1.61E-05	9.57
*NH_2	-7.57E-06	9.92
*NH_3	-5.27E-08	10.17

Notes and references

1. Y. Wan, Z. Wang, J. Li and R. Lv, *ACS Nano*, 2022, **16**, 643-654.
2. Y. Gu, B. Xi, W. Tian, H. Zhang, Q. Fu and S. Xiong, *Adv Mater*, 2021, **33**, e2100429.
3. .
4. Y. Zhao, F. Li, W. Li, Y. Li, C. Liu, Z. Zhao, Y. Shan, Y. Ji and L. Sun, *Angew Chem Int Ed Engl*, 2021, **60**, 20331-20341.
5. M. I. Ahmed, C. Liu, Y. Zhao, W. Ren, X. Chen, S. Chen and C. Zhao, *Angew Chem Int Ed Engl*, 2020, **59**, 21465-21469.
6. Y. Fu, T. Li, G. Zhou, J. Guo, Y. Ao, Y. Hu, J. Shen, L. Liu and X. Wu, *Nano Lett*, 2020, **20**, 4960-4967.
7. A. Liu, M. Gao, Y. Gao, X. Ren, Y. Yang, Q. Yang, Y. Li, L. Gao, X. Liang and T. Ma, *Inorganic Chemistry Communications*, 2020, **120**.
8. K. Qian, L. Du, X. Zhu, S. Liang, S. Chen, H. Kobayashi, X. Yan, M. Xu, Y. Dai and R. Li, *Journal of Materials Chemistry A*, 2019, **7**, 14592-14601.
9. H. Jin, L. Li, X. Liu, C. Tang, W. Xu, S. Chen, L. Song, Y. Zheng and S. Z. Qiao, *Adv Mater*, 2019, **31**, e1902709.
10. Y. Ling, F. M. D. Kazim, S. Ma, Q. Zhang, K. Qu, Y. Wang, S. Xiao, W. Cai and Z. Yang, *Journal of Materials Chemistry A*, 2020, **8**, 12996-13003.
11. Y. Gu, B. Xi, W. Tian, H. Zhang, Q. Fu and S. Xiong, *Advanced Materials*, 2021, **33**, 2100429.
12. L. Luo, B. Wang, J. Wang and X. Niu, *Phys Chem Chem Phys*, 2021, **23**, 16658-16663.
13. Y. Liu, Y. Su, X. Quan, X. Fan, S. Chen, H. Yu, H. Zhao, Y. Zhang and J. Zhao, *ACS Catalysis*, 2018, **8**, 1186-1191.
14. Y. Zhang, J. Hu, C. Zhang, A. T. F. Cheung, Y. Zhang, L. Liu and M. K. H. Leung, *International Journal of Hydrogen Energy*, 2021, **46**, 13011-13019.
15. L. Shi, S. Bi, Y. Qi, R. He, K. Ren, L. Zheng, J. Wang, G. Ning and J. Ye, *ACS Catalysis*, 2022, **12**, 7655-7663.